Astigmatic Detection System with Feedback Mechanism for Calibrating Driving Waveform of Piezoelectric Actuators

Liao, Hsien Shun; Guo, Zheng Rong; Tan, Hong Sheng; Huang, Kuang Yuh; Hwang, Ing Shouh; Hwu, En Te

Published in:
IEEE Transactions on Instrumentation and Measurement

Link to article, DOI:
10.1109/TIM.2023.3300412

Publication date:
2023

Document Version
Peer reviewed version

Citation (APA):
Liao, H. S., Guo, Z. R., Tan, H. S., Huang, K. Y., Hwang, I. S., & Hwu, E. T. (2023). Astigmatic Detection System with Feedback Mechanism for Calibrating Driving Waveform of Piezoelectric Actuators. *IEEE Transactions on Instrumentation and Measurement*, *72*, Article 1007907. https://doi.org/10.1109/TIM.2023.3300412

Astigmatic Detection System with Feedback Mechanism for Calibrating Driving Waveform of Piezoelectric Actuators

Hsien-Shun Liao, Zheng-Rong Guo, Hong-Sheng Tan, Kuang-Yuh Huang, Ing-Shouh Hwang, and En-Te Hwu

Abstract: **Piezoelectric actuators are used extensively in precision measurement, manufacturing, and manipulation owing to their high resolution, rapid response, and considerable force output. However, the nonlinear characteristics of piezoelectric materials, including hysteresis and creep, increase the complexity to achieve accurate positioning. Common methods rely on creating an inverse model of the actuator to enable linear movement. This study presents a novel calibration method based on an astigmatic detection system for directly measuring the calibrated driving waveform. This method can be applied to various types of piezoelectric actuators and does away with the need for complicated modeling and parameter identification. The experiment section demonstrates the calibration process of a piezoelectric XYZ scanner. The test results reveal that the linearity of the XYZ scanner, driven by the calibrated driving waveforms, closely approximates that of a commercial closed-loop nanopositioner. Additionally, atomic force microscopy images verify that the proposed method significantly mitigates the image distortion caused by the nonlinear behavior of the piezoelectric material.**

Index Terms—**Astigmatism, non-linearity calibration, piezoelectric actuator.**

This work was financially supported by the National Science and Technology Council of Taiwan (MOST 111-2221-E-002-162 and NSTC 112-2221-E-002-246) and the LEO Foundation (Grant No. LF-OC-20-000370).
(Corresponding author: H.-S. Liao)

H.-S. Liao, Z.-R. Guo, H.-S. Tan, and K.-Y. Huang are with the Department of Mechanical Engineering, National Taiwan University, Taipei 10617, Taiwan (e-mail: liaohs@ntu.edu.tw; alan.850221@gmail.com; r11522646@ntu.edu.tw; kyhuang@ntu.edu.tw).

I.-S. Hwang is with the Institute of Physics, Academia Sinica, Taipei 11529, Taiwan (e-mail: ishwang@phys.sinica.edu.tw).

E.-T. Hwu is with the Department of Health Technology, Technical University of Denmark, Lyngby 2800, Denmark (e-mail: etehw@dtu.dk).

I. INTRODUCTION

PIEZOELECTRIC actuators can generate rapid and precise displacement through the application of a voltage driving due to the inverse piezoelectric effect [1]. These advantages have led to their widespread use in various fields, such as precision measurement, manufacturing, and manipulation [2]–[5]. Furthermore, different types of piezoelectric actuators have been developed, including piezotube, flexure-guided, and friction-inertia actuators, to meet various performance requirements [6]–[10]. Nevertheless, nonlinear relationships are present in all piezoelectric actuators. Due to hysteresis and creep phenomena, the relationship between the driving signal and displacement is nonlinear, which complicates the attainment of accurate positioning [11], [12].

Calibrations for nonlinearity often involves constructing a mathematical model of the piezoelectric actuator and deriving a driving waveform from the inverse model to enable linear displacement [13]–[15]. However, this approach requires complicated modeling and accurate system identification, both of which can vary depending on the piezoelectric material and actuator design. Another common method features a real-time closed-loop controller with an additional displacement sensor [16]–[18]. However, the response speed of the closed-loop method is slower than that of the open-loop method due to the additional feedback latency. Moreover, the gain values of the controller must be optimized based on the operating conditions. The noise and sensitivity of the displacement sensor can affect positioning precision, often resulting in lower resolution than an open-loop control system. The displacement sensor and the closed-loop controller also increase the cost, size, and complexity of the positioning system [13], [19].

In this study, we propose a novel calibration method and a homemade calibration system with a feedback mechanism to directly measure the calibrated driving waveform. Once the calibrated driving waveform is obtained, the piezoelectric actuator can perform linear movement under open-loop control. This eliminates the need for a closed-loop controller and displacement sensor, allowing the piezoelectric actuator to benefit from high-speed, low noise, low cost, and reduced complexity. Moreover, since the calibrated driving waveform is directly obtained through measurement, the requirement for complicated system modeling and identification is circumvented. Lastly, the proposed calibration system can be conveniently applied to different types of piezoelectric actuators, providing a rapid, straightforward calibration process.

II. Method And Instrumentation

A. Calibration Method for Driving Waveform

Fig. 1 illustrates the proposed method for measuring the calibrated driving waveform of the piezoelectric actuator. This method requires a closed-loop nanopositioner to hold the piezoelectric actuator. The nanopositioner is driven by a function generator that uses a triangular waveform signal, V_{tri}, to provide a linear displacement, D_{stage}. The piezoelectric actuator, driven by a feedback controller, generates an inverse movement, $D_{actuator}$, to compensate for the D_{stage}. As a result, the total displacement, D_{total}, remains constant and is measured using a displacement sensor. The feedback controller captures the displacement signal, V_{total}, and maintains it at 0 V by regulating the piezoelectric actuator. Thus, the calibrated driving waveform, V_{cal}, of the piezoelectric actuator can generate a linear movement.

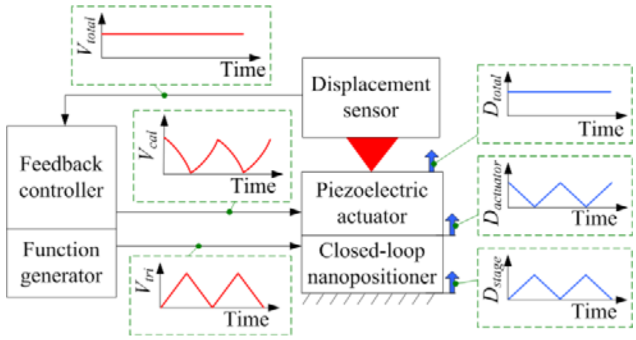

Fig. 1. Illustration of the proposed method for measuring the calibrated driving waveform.

B. Astigmatic Detection System

The astigmatic detection method is widely used in digital-versatile-disk pickup heads, offering advantages such as high speed, small laser spot, compact size, and low cost [20]–[23]. In this study, we employed a commercial astigmatic pickup head as the displacement sensor for calibration. Fig. 2(a) illustrates a typical optical configuration of the pickup head. A collimated laser beam is focused on a measured sample through an objective lens. The reflected beam from the sample is detected by a photodetector-integrated chip (PDIC) after passing through an astigmatic lens such as a cylinder lens. The shape of the laser spot on the PDIC changes with the vertical position of the sample due to the astigmatism, as illustrated in Fig. 2(b). The focus error signal (FES), defined in Equation 1, can detect the vertical displacement of the sample:

$$\mathrm{FES} = (S_A + S_C) - (S_B + S_D). \tag{1}$$

where S_A, S_B, S_C, and S_D are the voltage signals from the corresponding four-quadrant photosensors A, B, C, and D. The relationship between the FES and the sample displacement is termed the S-curve. When the sample surface is in the focal plane of the pickup head, the laser spot on the PDIC is circular, and the corresponding FES is 0 V. The FES is proportional to the sample displacement in the linear region of the S-curve. Hence, the FES voltage can be converted to displacement after the sensitivity $\Delta V/\Delta Z$ is calibrated using the closed-loop nanopositioner to provide a known displacement.

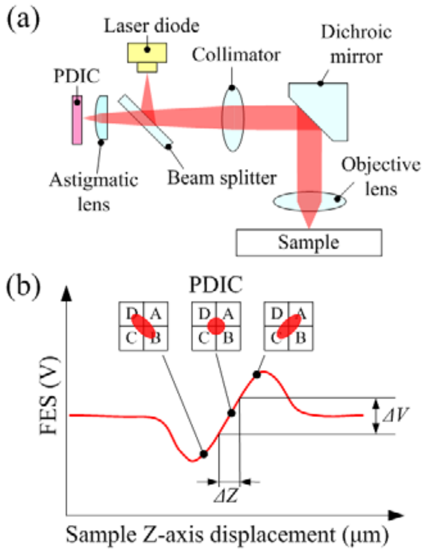

Fig. 2. Illustration of the (a) optical configuration and (b) S-curve of the astigmatic pickup head.

C. Calibration System Design

Figs. 3(a) and 3(b) illustrate the system configuration and mechanical design of the proposed calibration system, respectively. A closed-loop vertical nanopositioner (P-611. ZS, Physik Instrumente), equipped with a built-in strain gauge sensor and piezo-servo controller (E-665. SR, Physik Instrumente), can execute the linear movement within a 100 µm range. In the closed-loop mode, it can achieve a resolution of 2 nm with a linearity error lower than 0.1%. The piezoelectric actuator under examination was affixed to this closed-loop nanopositioner. The total displacement of the piezoelectric actuator and closed-loop nanopositioner in the vertical direction was measured using an astigmatic pickup head (TOP1100s, TopRay Technologies). The pickup head was maneuvered to its working distance on the piezoelectric actuator using a manual XYZ stage. Given the short working distance of the pickup head (1.28 mm) and its slim dimensions (48.7 mm × 36.7 mm × 7.5 mm), its objective lens was relocated to a lens holder at an appropriate distance from the pickup head to prevent physical contact between the pickup head and the piezoelectric actuator. A custom-made pickup head amplifier (TOP1100s driving circuit, OME Technology) generated the FES. It was calibrated to present the total displacement of the piezoelectric actuator and closed-loop nanopositioner. The calibration system was controlled by a programmable controller (PXIe system, National Instruments), which includes a chassis (PXIe-1062Q), a real-time controller (PXIe-8840), and two field-programmable gate array (FPGA) modules (PXIe-7961R) with adapters (NI5781). An FPGA module served as a function generator, generating a triangular signal to the piezo-servo controller of the closed-loop nanopositioner to induce linear movement. The other FPGA module was programmed as a proportional–integral–derivative (PID) controller with a 25-ns loop time, which acquired the FES and produced the driving signal for the piezoelectric actuator to maintain the FES at 0 V. The programmable controller also recorded the driving signal as a calibrated driving waveform, which was amplified by a high voltage amplifier (PD200, PiezoDrive) to stimulate the piezoelectric material. In addition to capturing the calibrated driving waveform, the calibration system verified the linearity of the piezoelectric actuator. For this purpose, the original objective lens of the astigmatic pickup head, with a numerical aperture (NA) of 0.6, was substituted with an objective lens (CAY033, Thorlabs) with an NA of 0.4. This substitution increased the measurable linear region from 6 µm to approximately 30 µm [24], [25]. However, there exists a trade-off between measurable range and sensitivity. The sensitivities with 0.6 and 0.4 NA objective lenses were 3.9 and 10.3 nm/mV, respectively, and the corresponding root mean square (RMS) noise values of the FES were 2.0 and 5.2 nm.

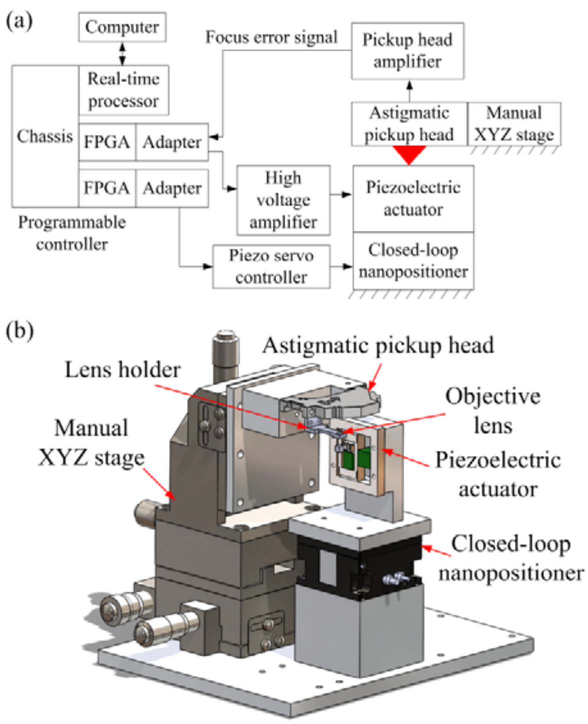

Fig. 3. (a) Block diagram and (b) mechanical design of the calibration system.

D. Piezoelectric Actuator and AFM

An XYZ scanner for high-speed atomic force microscopy (HS-AFM) was selected as the piezoelectric actuator for linearity calibration [26]–[28]. Fig. 4(a) illustrates the flexture-guided structure of the XYZ scanner, boasting advantages such as compact size and high response bandwidth. Although the XYZ scanner's application in imaging the formation processes of nanobubbles and high-speed force mapping has been demonstrated in the literature [27], [28], previous studies have reported that the hysteresis nonlinearity of the XYZ scanner induces image distortion. For the *X*-axis displacement calibration, the XYZ scanner was mounted on a vertical holder to fit the measurement orientation of the calibration system, as shown in Fig. 4(b). For the *Y*-axis calibration, the XYZ scanner was remounted with the *Y*-axis oriented upward. A cube equipped with mirrors was affixed to the XYZ scanner to enhance the measurement sensitivity of the astigmatic pickup head.

To illustrate the performance post-calibration, the XYZ scanner was integrated into a custom AFM system, as shown in Fig. 4(c) [28]. An astigmatic pickup head, similar to that used in the calibration system, was employed to detect cantilever deflection. A lock-in amplifier (SR830, Stanford Research) generated the excitation signal for the cantilever and detected its amplitude. The same PXIe controller employed in the calibration system was reprogrammed to perform AFM functions, such as *Z*-axis feedback control and *XY*-axis scanning. Triangular and calibrated driving waveforms were employed for *XY*-axis scanning for comparison.

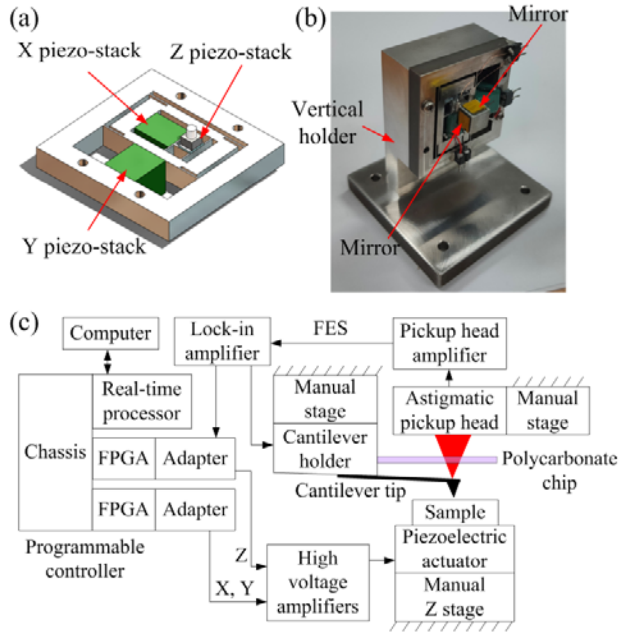

Fig. 4. (a) Structure of the XYZ scanner. (b) Photograph of XYZ scanner mounted on vertical holder for calibration. (c) AFM system configuration.

III. Results And Discussion

A. Driving Waveform Calibration

The calibrated waveform measurement involved a closed-loop nanopositioner controlled by a triangular waveform; The nanopositioner performed a reciprocated motion with a travel distance of 7 μm. To compensate for the displacement of the closed-loop scanner, the XYZ scanner was managed by the

PID controller. Figs. 5(a) and 5(c) present the calibrated driving waveforms for the *X*- and *Y*-axes, respectively. Both the *X*- and *Y*-axes calibrated driving waveforms were nonlinear. Moreover, the voltage range of the *Y*-axis waveform, as illustrated in Fig. 5(c), was lower than that of the *X*-axis waveform shown in Fig. 5(a) due to the *Y*-axis scanner's larger travel range compared with the *X*-axis scanner. Figs. 5(b) and 5(d) depict the calibrated FESs corresponding to Figs. 5(a) and 5(c), representing the total displacement in the *X* and *Y* directions, respectively. The results indicate that the total displacement signals of both axes can be maintained at approximately a position of 0 nm, which corresponds to the focal position of the pickup head. Therefore, the XYZ scanner's movement was linear when the calibrated driving waveform was used.

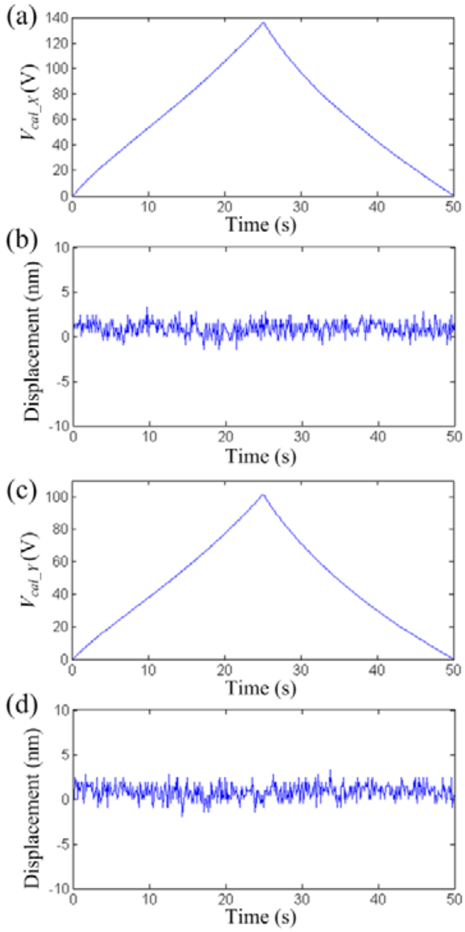

Fig. 5. (a) Calibrated driving waveform for the *X*-axis. (b) Total displacement in the *X*-direction. (c) Calibrated driving waveform for the *Y*-axis. (d) Total displacement in the *Y*-direction.

B. Linearity Verification Using Astigmatic Pickup Head

The calibration system, based on the astigmatic pickup head, was employed to determine the linearity of the XYZ scanner. Initially, the displacement of the closed-loop scanner was measured as a reference. The closed-loop nanopositioner, driven by a triangular waveform, was the focus of measurement, while the XYZ scanner remained stationary. Thus, the displacement of the closed-loop nanopositioner is represented by the FES of the astigmatic pickup head. Fig. 6(a) depicts the *X*-axis displacement signal of the closed-loop nanopositioner. To evaluate linearity, the coefficient of determination R^2 was calculated using the Matlab linear fitting function [29]. The average R^2 of the forward and backward movements was 0.9991, thereby indicating the linear displacement of the closed-loop nanopositioner. For the XYZ scanner examination, the closed-loop nanopositioner remained stationary, whereas the XYZ scanner was driven by triangular and calibrated waveforms. The blue dashed and red solid lines in Fig. 6(b) represent the displacement signals obtained using the triangular and calibrated waveforms, respectively. The displacement signal with the triangular driving waveform exhibited evident nonlinear hysteresis, resulting in a lower R^2 of 0.9950. Conversely, the displacement with the calibrated driving waveform yielded an R^2 of 0.9993, showing linearity comparable to the closed-loop nanopositioner. Similar to the *X*-axis, the *Y*-axis displacement of the closed-loop scanner also boasted a high R^2 of 0.9996, as illustrated in Fig. 6(c). As shown in Fig. 6(d), the *Y*-axis displacement signals of the XYZ scanner, driven by triangular and calibrated waveforms, had R^2 values of 0.9929 and 0.9994, respectively. These results further validate the high degree of linearity achieved by the calibrated waveform, akin to that of the closed-loop nanopositioner.

To assess the repeatability of the XYZ scanner, the linearity measurements were replicated 100 times consecutively within a 6-minute window. Figs. 7(a) and 7(b) represent the R^2 of the 100 measurements in the *X*- and *Y*-directions, respectively. The blue dotted lines and the red solid lines depict the results obtained using triangular and calibrated waveforms, respectively. The results demonstrate that the XYZ scanner maintained stable linearity during the continual measurements, with maximum R^2 variations lower than 0.001 and 0.0002 for the triangular and calibrated waveforms, respectively. The statistical results of 100 measurements, including R^2, the sum of squared error (SSE), and the RMS error (RMSE), are listed in Table I. The standard deviation (SD) of R^2 with the calibrated waveform was also lower than that with the triangular waveform in both the *X*- and *Y*-directions.

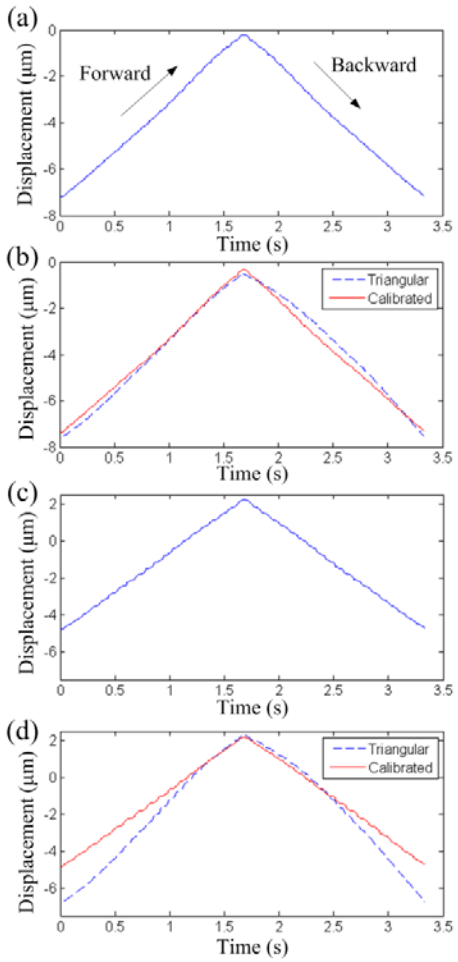

Fig. 6. Displacement signals of the closed-loop nanopositioner with triangular driving waveform in the (a) *X*-axis and (c) *Y*-axis directions. Displacement signals of the XYZ scanner driven by triangular and calibrated waveforms: (b) *X*-axis and (d) *Y*-axis.

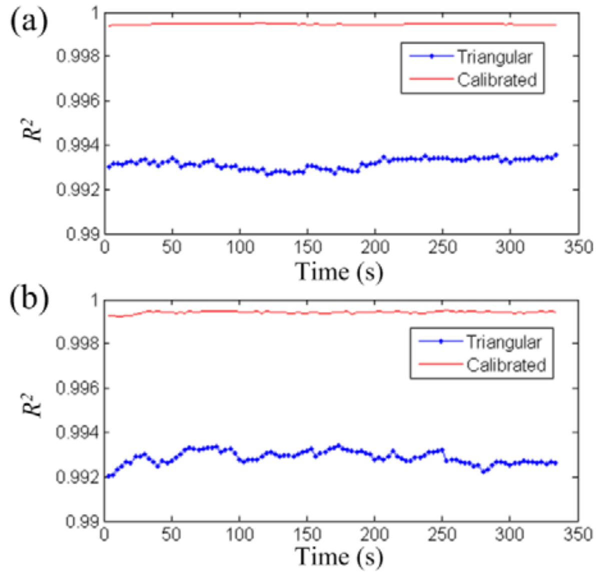

Fig. 7. Repeated measurements of R^2 using the triangular and calibrated waveforms: (a) *X*-axis and (b) *Y*-axis.

TABLE I

RESULTS OF REPEATED MEASUREMENTS

Axis	Driving waveform	R^2 (mean ± SD)	SSE (mean ± SD)	RMSE (mean ± SD)
X	Triangular	0.9932 ± 2.3e-4	0.1287 ± 0.0038	0.0222 ± 2.9e-4
	Calibrated	0.9995 ± 2.1e-5	0.0030 ± 1.3e-4	0.0039 ± 8.7e-5
Y	Triangular	0.9929 ± 2.9e-3	0.0839 ± 0.0032	0.0166 ± 3.5e-4
	Calibrated	0.9994 ± 5.1e-5	4.8472e-4 ± 4.4e-5	0.0022 ± 9.6e-5

C. AFM Imaging

To illustrate AFM imaging with the XYZ scanner, a standard grating sample (TGQ1, NT-MDT) was used for scanning. The grating sample featured 20-nm height square structures with a 3-μm period. An AFM probe (AC240TS, Olympus) was used to scan the sample surface in tapping mode, operating at a resonant frequency of 71.3 kHz. The scan covered an area of 7.4 μm × 7.4 μm at an image resolution of 256 × 256 pixels, with a scan rate of 0.3 lines/s. Height images generated by scanning with triangular waveforms in forward and backward directions are depicted in Figs. 8(a) and 8(b), respectively. The images reveal that the triangular driving waveform induced significant image distortion, which resulted in an elongation of the square structures on the right side in the *X*-direction and the upper side in the *Y*-direction. Conversely, Figs. 8(c) and 8(d) present the forward and backward scan images acquired using calibrated driving waveforms. Compared with the images in Figs. 8(a) and 8(b), the size and period of the square structures appear more uniform in the X and Y directions in Figs. 8(c) and 8(d). These results demonstrate that the calibrated driving waveform enables the XYZ scanner to execute high-resolution linear movements.

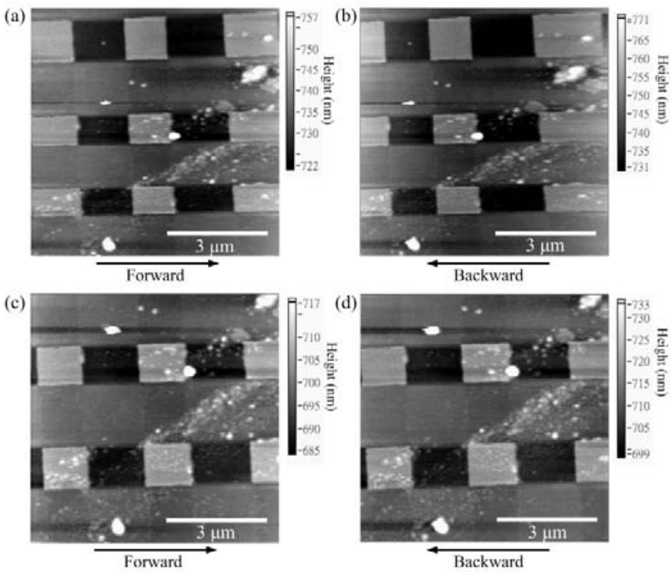

Fig. 8. AFM height images obtained by scanning with triangular driving waveforms in (a) forward and (b) backward directions. AFM height images acquired by scanning with calibrated driving waveforms in (c) forward and (d) backward directions.

IV. Summary

This study presented a novel calibration technique designed to address the nonlinearity inherent in piezoelectric actuators. The method utilizes a closed-loop nanopositioner to generate linear motion and employs a feedback controller to guide the piezoelectric actuator to compensate for this linear movement. Consequently, the calibrated driving waveform for the piezoelectric actuator is obtained directly, eliminating the need for modeling and system identification. Furthermore, the study showcased a calibration system designed around an astigmatic pickup head for calibrating an AFM XYZ scanner. This versatile calibration system can be adapted for various types of piezoelectric actuators and can also be expanded for three-dimensional measurements by incorporating three pickup heads and an XYZ closed-loop nanopositioner. This system can also verify the linearity of the piezoelectric actuator. The empirical results underscore that the linearity of the XYZ scanner closely mirrors that of the commercial closed-loop nanopositioner when the calibrated driving waveform is used. The experimental data from AFM demonstrate that the proposed method can effectively alleviate image distortion stemming from the nonlinearity of piezoelectric material.

References

[1] S. Mohith, A. R. Upadhya, K. P. Navin, S. M. Kulkarni, and M. Rao, “Recent trends in piezoelectric actuators for precision motion and their applications: a review,” *Smart Mater. Struct.,* vol. 30, no. 1, Dec. 2020, Art. no. 013002.

[2] G. Schitter, K. J. Astrom, B. E. DeMartini, P. J. Thurner, K. L. Turner, and P. K. Hansma, “Design and modeling of a high-speed AFM-scanner,” *IEEE Trans. Control Syst. Technol.,* vol. 15, no. 5, pp. 906-915, Sep. 2007.

[3] J. Jung and K. Huh, “Simulation tool design for the two-axis nano stage of lithography systems,” *Mechatronics,* vol. 20, no. 5, pp. 574-581, Aug. 2010.

[4] S. K. Nah and Z. W. Zhong, “A microgripper using piezoelectric actuation for micro-object manipulation,” *Sens. Actuator A,* vol. 133, no. 1, pp. 218-224, Jan. 2007.

[5] E. T. Hwu *et al.*, “Design and characterization of a compact nano-positioning system for a portable transmission x-ray microscope,” *Rev. Sci. Instrum.,* vol. 84, no. 12, Dec. 2013, Art. no. 123702.

[6] D. Habineza, M. Rakotondrabe, and Y. L. Gorrec, "Bouc–wen modeling and feedforward control of multivariable hysteresis in piezoelectric systems: application to a 3-dof piezotube scanner," *IEEE Trans. Control Syst. Technol.,* vol. 23, no. 5, pp. 1797-1806, Sep. 2015.

[7] S. Fukuda, T. Uchihashi, and T. Ando, "Method of mechanical holding of cantilever chip for tip-scan high-speed atomic force microscope," *Rev. Sci. Instrum.,* vol. 86, no. 6, Jun. 2015, Art. no. 063703.

[8] C.-L. Chen and S.-K Hung, "Visual servo control system of a piezoelectric 2-degree-of-freedom nano-stepping motor," *Micromachines,* vol. 10, no. 12, Nov. 2019, Art. no. 811.

[9] W.-M. Wang, K.-Y Huang, H.-F. Huang, I.-S. Hwang, and E.-T. Hwu, "Low-voltage and high-performance buzzer-scanner based streamlined atomic force microscope system," *Nanotechnology*, vol. 24, no. 45, Oct. 2013, Art. no. 455503.

[10] H. S. Liao *et al.*, "Low-cost, open-source XYZ nanopositioner for high-precision analytical applications," *HardwareX,* vol. 11, Apr. 2022, Art. no. e00317.

[11] J. Gan and X. Zhang, "A Review of nonlinear hysteresis modeling and control of piezoelectric actuators," *AIP Adv.,* vol. 9, no. 4, Apr. 2019, Art. no. 040702.

[12] D. V. Sabarianand, P. Karthikeyan, and T. Muthuramalingam, "A review on control strategies for compensation of hysteresis and creep on piezoelectric actuators based micro systems," *Mech. Syst. Signal Process.,* vol. 140, Jun. 2020, Art. no. 106634.

[13] R. Changhai and S. Lining, "Hysteresis and creep compensation for piezoelectric actuator in open-loop operation," *Sens. Actuator A,* vol. 122, no. 1, pp. 124-130, Jul. 2005.

[14] Y. Qin, Y. Tian, D. Zhang, B. Shirinzadeh, and S. Fatikow, "A novel direct inverse modeling approach for hysteresis compensation of piezoelectric actuator in feedforward applications," *IEEE ASME Trans. Mechatron.,* vol. 18, no. 3, pp. 981-989, Jun. 2013.

[15] Z. Nie, Y. Cui, J. Huang, Y. Wang, and T. Chen, "Precision open-loop control of piezoelectric actuator," *J. Intell. Mater. Syst. Struct.,* vol. 33, no. 9, pp. 1198-1214, May. 2022.

[16] U. Bhagat, B. Shirinzadeh, Y. Tian, and D. Zhang, "Experimental analysis of laser interferometry-based robust motion tracking control of a flexure-based mechanism," *IEEE Trans. Autom. Sci. Eng.,* vol. 10, no. 2, pp. 267-275, Apr. 2013.

[17] C. Zhou *et al.*, "A closed-loop controlled nanomanipulation system for probing nanostructures inside scanning electron microscopes," *IEEE ASME Trans. Mechatron.,* vol. 21, no. 3, pp. 1233-1241, Feb. 2016.

[18] C. Rusu, S. Besoiu, and M. O. Tatar, "Design and closed-loop control of a piezoelectric actuator," *IOP Conf. Ser. Mater. Sci. Eng.,* vol. 1018, no. 1, 2021, Art. no. 012002.

[19] B. Borovic, A. Q. Liu, D. Popa, H. Cai, and F. L. Lewis, "Open-loop versus closed-loop control of MEMS devices: choices and issues," *J. Micromech. Microeng.,* vol. 15, no. 10, pp. 1917-1924, Aug. 2005.

[20] K.-C. Fan, C.-L. Chu, J.-L. Liao, and J.-I. Mou, "Development of a high-precision straightness measuring system with DVD pick-up head," *Meas. Sci. Technol.,* vol. 14, no. 1, pp. 47-51, Nov. 2002.

[21] E.-T. Hwu, S.-K. Hung, C.-W. Yang, I.-S. Hwang, and K.-Y. Huang, "Simultaneous detection of translational and angular displacements of micromachined elements," *Appl. Phys. Lett.*, vol. 91, no. 22, Nov. 2007, Art. no. 221908.

[22] E.-T. Hwu, S.-K. Hung, C.-W. Yang, K.-Y. Huang, and I.-S. Hwang, "Real-time detection of linear and angular displacements with a modified DVD optical head," *Nanotechnology*, vol. 19, no. 11, Feb. 2008, Art. no. 115501.

[23] Q. Vo, F. Fang, X. Zhang, and L. Zhu, "Reducing the residual focus error signal in optical pickup head astigmatism displacement systems using the signal conditioning method," *Appl. Optics*, vol. 57, no. 34, pp. 9972-9980, Nov. 2018.

[24] E. T. Hwu, K.-Y. Huang, S.-K. Hung, and I.-S Hwang, "Measurement of cantilever displacement using a compact disk/digital versatile disk pickup head," *Jpn. J. Appl. Phys.*, vol. 45, No. 3B, pp. 2368-2371, Mar. 2006.

[25] E. T. Hwu *et al.*, "High-performance spinning device for DVD-based micromechanical signal transduction," *J. Micromech. Microeng.*, vol. 23, no. 4, Mar. 2013, Art. No. 045016.

[26] H. S. Liao *et al.*, "High-speed atomic force microscope based on an astigmatic detection system," *Rev. Sci. Instrum.,* vol. 85, no. 10, Oct. 2014, Art. no. 103710.

[27] H.-S. Liao, K. K. Lei, and Y. F. Tseng, "High-speed force mapping based on an astigmatic atomic force microscope," *Meas. Sci. Technol.,* vol. 30, no. 2, Jan. 2019, Art. no. 027002.

[28] H.-S. Liao, C.-W. Yang, H.-C. Ko, E.-T. Hwu, and I.-S. Hwang, "Imaging initial formation processes of nanobubbles at the graphite–water

interface through high-speed atomic force microscopy," *Appl. Surf. Sci.,* vol. 434, pp. 913-917, Mar. 2018.

[29] J. A. Cornell and R. D. Berger, "Factors that influence the value of the coefficient of determination in simple linear and nonlinear regression models," *Phytopathology*, vol. 77, no. 1, pp. 63-70, 1987.